Self-consistent meta-generalized gradient approximation within the projector-augmented-wave method

Jianwei Sun, Martijn Marsman, Gábor I. Csonka, Adrienn Ruzsinszky, Pan Hao, Yoon-Suk Kim, Georg Kresse, and John P. Perdew

Phys. Rev. B **84**, 035117 — Published 22 July 2011

DOI: 10.1103/PhysRevB.84.035117

Selfconsistent Meta-Generalized Gradient Approximation within the Projector-Augmented-Wave Method

Jianwei Sun,[1] Martijn Marsman,[2] Gábor I. Csonka,[3] Adrienn Ruzsinszky,[1]
Pan Hao,[1] Yoon-Suk Kim,[2] Georg Kresse,[2] and John P. Perdew[1]

[1]*Department of Physics and Quantum Theory Group, Tulane University, New Orleans, Louisiana 70118, USA*

[2]*University of Vienna, Faculty of Physics and Center for Computational Materials Science, Sensengasse 8/12, A-1090 Wien, AUSTRIA*

[3]*Department of Inorganic and Analytical Chemistry, Budapest University of Technology and Economics, H-1521 Budapest, HUNGARY*

Abstract

The Tao-Perdew-Staroverov-Scuseria (TPSS) meta-generalized-gradient-approximation (MGGA) and its revised version, the revTPSS, are implemented self-consistently within the framework of the projector-augmented-wave (PAW) method, using a plane wave basis set. Both TPSS and revTPSS yield accurate atomization energies for the molecules in the AE6 set, better than those of the standard Perdew-Burke-Ernzerhof (PBE) generalized-gradient-approximation. For lattice constants and bulk moduli of 20 diverse solids, revTPSS performs much better than PBE, and on average as well as PBEsol and Armiento-Mattsson (AM05), GGAs designed for solids. The latter two overestimate the atomization energies for molecules to an unacceptable degree. However, the revTPSS presents only a slight improvement over PBEsol for the prediction of cohesive energies for solids, and some deterioration with respect to PBE. We also study the magnetic properties of Fe, for which both TPSS and revTPSS predict the right ground-state solid phase, the ferromagnetic body-centered-cubic (bcc) structure, with an accurate magnetic moment.

I. INTRODUCTION

In the last decades, Kohn-Sham (KS) density functional theory (DFT)[1–3] has proven to be a very powerful tool in condensed matter physics and quantum chemistry. The key ingredient within KS-DFT, the exchange-correlation energy $E_{\rm xc}$ as a functional of the electron spin densities $n_\uparrow(\mathbf{r})$ and $n_\downarrow(\mathbf{r})$, must be approximated. Semilocal approximations (e.g., Refs.[4–7]) of the form

$$E_{\rm xc}[n_\uparrow, n_\downarrow] = \int d^3r n\epsilon_{\rm xc}(n_\uparrow, n_\downarrow, \nabla n_\uparrow, \nabla n_\downarrow, \tau_\uparrow, \tau_\downarrow) \tag{1}$$

require only a single integral over real space and so are practical even for large molecules or unit cells. In Eq. (1) $n_\uparrow$ and $n_\downarrow$ are the electron densities of spin $\uparrow$ and $\downarrow$, respectively, $\nabla n_{\uparrow,\downarrow}$ the local gradients of the spin densities, $\tau_{\uparrow,\downarrow} = \sum_k |\nabla\psi_{k\uparrow,\downarrow}|^2/2$ the kinetic energy densities of the occupied KS orbitals $\psi_{k\sigma}$ of spin σ, and $\epsilon_{\rm xc}$ the approximate exchange-correlation energy per electron. All equations are in atomic units.

The semilocal approximations include three rungs of the so-called Jacob's ladder in DFT[8]: local spin density approximation (LSDA), generalized gradient approximation (GGA), and meta-GGA (MGGA). The lowest rung, the LSDA[1,4], uses only the densities $n_\uparrow$ and $n_\downarrow$ as ingredients, is exact for a uniform electron gas, and predicts reasonable but too-short lattice constants for solids, good surface energies for simple metals (but with substantial error cancellation between exchange and correlation), and molecular atomization energies that are unacceptably high. Compared to the LSDA, GGAs with standard[5] or diminished[9] gradient dependences include additional semilocal information, the gradients of the spin densities. With the advent of GGAs[5,10–17], density functional theory has become popular not only in solid state physics, but also in quantum chemistry. However, the accuracy of the commonly used GGAs is still limited. For example, the nonempirical Perdew-Burke-Ernzerhof (PBE) GGA[5] predicts reasonable but too-long lattice constants, surface energies that are better than LSDA for exchange alone and correlation alone but worse for their sum, and improved atomization energies to an error level of about 10 kcal/mol. Since the commonly used GGAs in general overcorrect the lattice constant with respect to LSDA, recent years have seen the emergence of "GGAs for solids" with diminished gradient dependences (e.g., AM05[18] and PBEsol[19]) which typically predict good lattice constants and surface energies, but rather poor atomization energies.

The MGGA is a natural way to improve accuracy further by making use of additional

semilocal information, e.g., the Laplacian of the density $\nabla^2 n_\sigma$ or the kinetic energy densities τ_σ. Usually, MGGA functionals include either the Laplacian of the density[20–22] or the kinetic energy density[6,7,23–27]. Some of them, however, include both $\nabla^2 n_\sigma$ and τ_σ[17,28,29]. There are two reasons for the inclusion of τ_σ as an alternative (or additional) inhomogeneity parameter to $\nabla^2 n_\sigma$. First, τ_σ arises naturally in the Taylor expansion of the exact spherically averaged exchange hole near the electron it surrounds[30]. Second, the use of τ_σ provides a simple and straightforward way to make a correlation functional exactly one-electron self-interaction free[31]. By using the kinetic energy density τ as an extra ingredient, MGGAs can distinguish between single-orbital-shape regions and orbitally-overlapped regions. In a single-orbital-shape region, $z = \tau_w/\tau = 1$, where $\tau_w = |\nabla n|^2/8n$ is the von Weizsäcker kinetic energy density, while $z = 0$ for the uniform electron gas where orbitals are highly overlapped. It has been proven strictly[32] that $0 \leq z \leq 1$ for all systems. Computationally, MGGAs are not much more expensive than LSDA or GGA[33,34]. In computations for molecules containing transition-metal atoms, the Tao-Perdew-Staroverov-Scuseria (TPSS)[6] MGGA is only 30% slower[34] than PBE.

By respecting two paradigms[6], the uniform electron gas for condensed matter physics and the hydrogen atom for quantum chemistry, the nonempirical TPSS MGGA predicts lattice constants that are only a little shorter and a little more accurate than those of PBE, good surface energies, and very good atomization energies[6,33]. Because selfconsistent implementations were not available in condensed matter codes and perhaps due to its lattice-constant errors, TPSS has not been so widely adopted. By restoring the second-order gradient expansion for exchange over a wide range of densities as the PBEsol[19] GGA did, and by respecting the paradigms of both condensed matter physics and quantum chemistry as the TPSS[6] did, the newly proposed revised TPSS (revTPSS)[7] unites the advantages of PBEsol and TPSS, giving good lattice constants, as well as good surface and atomization energies. revTPSS has already been implemented nonselfconsistently in VASP[7], BAND[7], and GPAW[35], and selfconsistently in GAUSSIAN[7]. Although rather accurate MGGA total energies and energy differences can often be found nonselfconsistently using LSDA or GGA orbitals, MGGA selfconsistency is needed for accurate and efficient MGGA forces and force-based geometry optimizations.

We recently applied self-consistent revTPSS to the problem of adsorption of a CO molecule on transition metal surfaces [36]. We found that, unlike all tested GGAs, the revTPSS

meta-GGA provides a good simultaneous prediction of the bulk lattice constant and surface energy of the metal, on the one hand, and of the adsorption energy on the other.

There is a second but more empirical and computationally more expensive way to preserve the good solid-state performance of the PBEsol GGA while improving the description of atoms and molecules: by hybridizing PBEsol exchange with exact exchange in a global[37] or range-separated[38] way. Other GGA's for solids, such as Ref. 18, could also be hybridized. Hybrid functionals will not be discussed further here.

This paper is organized as follows. Section II presents the self-consistent implementation of the TPSS and revTPSS MGGAs within the projector augmented wave (PAW) method. Section III provides computational details. Results for the atomization energies of the molecules in the AE6 set, the lattice constants, bulk moduli, and cohesive energies of a test set of 20 solids, and the magnetic moment of Fe and Ni, are given in Section IV. Virial stresses as a test of selfconsistency are examined at the beginning of Section IV B. Finally, conclusions are drawn in Section V.

II. SELF-CONSISTENT IMPLEMENTATION OF MGGA WITHIN THE PROJECTOR AUGMENTED-WAVE (PAW) METHOD

In the Kohn-Sham (KS) auxiliary non-interacting system, electrons move in an effective potential (where, for the sake of simplicity, spins are suppressed in the expressions):

$$v_{\rm eff}(\mathbf{r}) = v_{\rm ext}(\mathbf{r}) + v_{\rm H}([n];\mathbf{r}) + v_{\rm xc}([n];\mathbf{r}). \tag{2}$$

Here $v_{\rm ext}(\mathbf{r})$ is the external potential,

$$v_{\rm H}([n];\mathbf{r}) = \frac{\delta E_{\rm H}[n]}{\delta n(\mathbf{r})} = \int d^3r' \frac{n(\mathbf{r}')}{|\mathbf{r}-\mathbf{r}''|} \tag{3}$$

is the Hartree potential, and

$$v_{\rm xc}([n];\mathbf{r}) = \frac{\delta E_{\rm xc}[n]}{\delta n(\mathbf{r})} \tag{4}$$

is the exchange-correlation potential. For exchange-correlation functionals which only involve the density n, its gradient ∇n, and its Laplacian $\nabla^2 n$, evaluation of the exchange-correlation potential can be easily performed[2]. However, the problem of deriving a potential becomes less clearcut for the τ-dependent MGGA, since the kinetic energy density τ is not known as an explicit functional of the electronic density. In the following, we will only

focus on the self-consistent implementation of the τ-dependent MGGAs, e.g., TPSS[6] and revTPSS[7].

There are two approaches[39] to deriving potentials from the MGGA exchange-correlation energies: (i) the optimized effective potential (OEP) method[40,41], which yields a local and multiplicative exchange-correlation potential (the same for all the orbitals), and (ii) the ansatz proposed by Neumann *et al*[42]. Because of its simplicity and because forces are readily available, we prefer the latter route. Method (ii) consists of making the total energy stationary with respect to orbital variations and yields a differential operator rather than a local, multiplicative KS potential. In this case, the expression $v_{\rm xc}^{\rm MGGA}(\mathbf{r})\psi_n(\mathbf{r})$ is replaced by:

$$\begin{aligned} v_{\rm xc}^{\rm MGGA}(\mathbf{r})\psi_n(\mathbf{r}) &= \frac{\delta E_{\rm xc}^{\rm MGGA}}{\delta n}\psi_n \\ &\rightarrow [\frac{\partial e_{\rm xc}^{\rm MGGA}}{\partial n} - \nabla\cdot(\frac{\partial e_{\rm xc}^{\rm MGGA}}{\partial \nabla n})]\psi_n - \frac{1}{2}\nabla\cdot\{\frac{\partial e_{\rm xc}^{\rm MGGA}}{\partial \tau}\nabla\psi_n\}, \end{aligned} \tag{5}$$

where $e_{\rm xc}^{\rm MGGA} = n\epsilon_{\rm xc}^{\rm MGGA}$ is the exchange-correlation energy density of a given MGGA. The resulting differential operator for $v_{\rm xc}^{\rm MGGA}(\mathbf{r})$ is:

$$\begin{aligned} v_{\rm xc}^{\rm MGGA}(\mathbf{r}) &\rightarrow [\frac{\partial e_{\rm xc}^{\rm MGGA}}{\partial n} - \nabla\cdot(\frac{\partial e_{\rm xc}^{\rm MGGA}}{\partial \nabla n})] - \frac{1}{2}\nabla\cdot\{\frac{\partial e_{\rm xc}^{\rm MGGA}}{\partial \tau}\nabla\} \\ &= v_{\rm xc}^{\rm GGA}(\mathbf{r}) - \frac{1}{2}\nabla\cdot\{\mu_{\rm xc}(\mathbf{r})\nabla\}, \end{aligned} \tag{6}$$

where

$$v_{\rm xc}^{\rm GGA}(\mathbf{r}) = [\frac{\partial e_{\rm xc}^{\rm MGGA}}{\partial n} - \nabla\cdot(\frac{\partial e_{\rm xc}^{\rm MGGA}}{\partial \nabla n})], \tag{7}$$

is of the usual form associated with GGAs[2], and

$$\mu_{\rm xc}(\mathbf{r}) = \frac{\partial e_{\rm xc}^{\rm MGGA}}{\partial \tau}. \tag{8}$$

is an additional contribution specific to τ-dependent MGGAs. Clearly, to arrive at a self-consistent implementation of the τ-dependent-MGGAs, it is necessary to derive the functional forms of $\partial e_{\rm xc}^{\rm MGGA}/\partial n$, $\partial e_{\rm xc}^{\rm MGGA}/\partial \nabla n$, and $\partial e_{\rm xc}^{\rm MGGA}/\partial \tau$. (See Appendices A and B for the TPSS and revTPSS MGGAs).

This approach was first proposed in Ref. 42 for the implementation of the BRx89 exchange functional[28]. The approximation of Eq. (5) results in a differential operator that deviates from the conventional (in real space) multiplicative Kohn-Sham potential (although the

operator is not fully nonlocal). Nevertheless, total energies obtained by this means are expected to be close to the proper KS result for most practical purposes. A similar generalized Kohn-Sham approach is routinely used for hybrid density functionals, where a fraction of the fully nonlocal Hartree-Fock potential is employed.

In the PAW method of Blöchl[43,44], the one-electron wave functions or orbitals are expanded in plane waves that see an ultra-soft pseudopotential, augmented by atom-centered partial waves. The construction usually begins with a free neutral reference atom for each element, spherical and spin-unpolarized due to fractional occupation numbers for orbitals in open subshells. For this reference atom, the Kohn-Sham equation (or rather a scalar-relativistic version thereof) is solved for a set of all-electron partial waves $\phi_i(\mathbf{r})$, each the product of a radial function and a spherical harmonic with angular momentum quantum numbers l, m, and energy quantum number ε. The all-electron partial waves are generated numerically on a radial grid, for the occupied orbital energies plus some higher energies chosen to describe scattering states. For each all-electron (AE) partial wave $\phi_i(\mathbf{r})$, an unnormalized pseudo (PS) partial wave $\tilde{\phi}_i(\mathbf{r})$ is constructed so that it coincides with $\phi_i(\mathbf{r})$ outside a radius r_c^l, and is smoothed inside as in Eq. (57) of Ref[44]. The core radius r_c^l is usually chosen to be approximately half the nearest-neighbor distance. Frozen core orbitals and unfrozen valence orbitals are then selected, where the latter will be allowed to respond to changes in the configuration or environment of the atom. Furthermore a local pseudopotential is constructed to describe the l quantum numbers that are not accounted for in the partial wave basis. The pseudopotential is then "unscreened" to produce a bare electron-ion pseudopotential, which transfers without modification from one approximation for $E_{\rm xc}[n]$ to another[45].

The AE valence orbital ψ_n is derived from the pseudo- (PS) orbital $\tilde{\psi}_n$ by means of a linear transformation:

$$|\psi_n\rangle = |\tilde{\psi}_n\rangle + \sum_i (|\phi_i\rangle - |\tilde{\phi}_i\rangle)\langle\tilde{p}_i|\tilde{\psi}_n\rangle. \tag{9}$$

The PS orbitals $\tilde{\psi}_n$ are the variational quantities of the PAW method and are expanded in plane waves. The index i is a shorthand for the atomic site $\mathbf{R}$, the angular momentum numbers $L = l, m$, and an additional index ε referring to the reference energy. By construction, the projector functions $\tilde{p}_i$ are dual to the PS valence partial waves:

$$\langle\tilde{p}_i|\tilde{\phi}_j\rangle = \delta_{ij}. \tag{10}$$

In the PAW method, the expectation value of any semilocal operator $\hat{A}$, e.g., the kinetic energy $-\frac{1}{2}\nabla^2$ and the electron density operator $|\mathbf{r}\rangle\langle\mathbf{r}|$, may be written as a plane-wave part plus a sum of non-plane-wave one-center corrections[46]:

$$\begin{aligned}\langle\hat{A}\rangle &= \sum_n f_n\langle\tilde{\psi}_n|\hat{A}|\tilde{\psi}_n\rangle + \sum_{n=1}^{N_c}\langle\tilde{\phi}_n^c|\hat{A}|\tilde{\phi}_n^c\rangle \\ &+ \sum_R\left(\sum_{i,j\in R}\rho_{ij}\langle\phi_j|\hat{A}|\phi_i\rangle + \sum_{n\in R}^{N_{c,R}}\langle\phi_n^c|\hat{A}|\phi_n^c\rangle\right) \\ &- \sum_R\left(\sum_{i,j\in R}\rho_{ij}\langle\tilde{\phi}_j|\hat{A}|\tilde{\phi}_i\rangle + \sum_{n\in R}^{N_{c,R}}\langle\tilde{\phi}_n^c|\hat{A}|\tilde{\phi}_n^c\rangle\right),\end{aligned} \tag{11}$$

where ρ_{ij} is a one-center density matrix, calculated from the pseudo-orbitals as:

$$\rho_{ij} = \sum_n f_n\langle\tilde{\psi}_n|\tilde{p}_i\rangle\langle\tilde{p}_j|\tilde{\psi}_n\rangle. \tag{12}$$

In Eq. (11), the f_n are the occupations of the valence states, and we have introduced the frozen core approximation in terms of N_c pseudo core states $\tilde{\phi}_n^c$, and the corresponding AE core states ϕ_n^c. The PS core states $\tilde{\phi}_n^c$, together with the PS valence states $\tilde{\phi}$, are determined by the Eq. (57) of Ref. 44. Here, only those parts that are specific to the TPSS and revTPPS MGGA approximation to the exchange-correlation energy and the Hamiltonian (the parts that involve the kinetic energy density) will be discussed.

Since the kinetic energy density is a semilocal quantity, it may be decomposed into three parts (analogously to the charge density in Eq. (18) of Ref. 44)

$$\tau + \tau_c = (\tilde{\tau} + \tilde{\tau}_c) + (\tau^1 + \tau_c^1) - (\tilde{\tau}^1 + \tilde{\tau}_c^1), \tag{13}$$

where $\tilde{\tau} = \sum_n f_n\frac{1}{2}|\nabla\tilde{\psi}_n|^2$ and $\tilde{\tau}_c = \sum_{n=1}^{N_c}\frac{1}{2}|\nabla\tilde{\phi}_n^c|^2$ are the kinetic energy density of the valence PS orbitals and the pseudo core kinetic energy density (first line of Eq. 11), respectively. The quantities τ^1, τ_c^1, and $\tilde{\tau}^1$, $\tilde{\tau}_c^1$ are the corresponding AE and PS one-center contributions (second and third line of Eq. (11), respectively). $\tilde{\tau}$ and $\tilde{\tau}_c$ are expanded in a plane wave basis set. All other contributions are represented on atom-centered logarithmic radial grids. The pseudo core kinetic energy densities $\tilde{\tau}_c$ and $\tilde{\tau}_c^1$ are equivalent to the AE kinetic energy density τ_c^1 outside a matching radius r_{pc} and continue smoothly onto τ_c^1 just inside the matching radius.

Analogously to Ref. 44, the exchange-correlation energy can be written as

$$E_{\rm xc} = E_{\rm xc}[\tilde{n} + \hat{n} + \tilde{n}_c, \tilde{\tau} + \tilde{\tau}_c] + \overline{E_{\rm xc}[n^1 + n_c^1, \tau^1 + \tau_c^1]} - \overline{E_{\rm xc}[\tilde{n}^1 + \hat{n} + \tilde{n}_c^1, \tilde{\tau}^1 + \tilde{\tau}_c^1]}, \quad (14)$$

where $\hat{n}$ is the compensation charge introduced to treat the long-range electrostatic interactions correctly, and $\overline{E}_{\rm xc}$ means that the corresponding quantity is evaluated on the atom-centered radial logarithmic grids[44]. The compensation charge $\hat{n}$ could be omitted in Eq. (14), since it has almost no effect on the results, but we retain it to make the calculation technically easier (via charge density mixing).

The expression for the Hamilton operator is similar to Eq. (47) of Ref. 44:

$$\tilde{H} = -\frac{1}{2}\nabla^2 + \tilde{v}_{\rm eff} + \tilde{\mu}_{\rm eff} + \sum_{(i,j)} |\tilde{p}_i\rangle (\hat{D}_{ij} + D_{ij}^1 - \tilde{D}_{ij}^1) \langle \tilde{p}_j|, \quad (15)$$

where

$$\begin{aligned} D_{ij}^1 &= \langle \phi_i| - \frac{1}{2}\nabla^2 + v_{\rm eff}^1 + \mu_{\rm eff}^1 |\phi_j\rangle \\ &= \langle \phi_i| - \frac{1}{2}\nabla^2 + v_{\rm eff}^1 |\phi_j\rangle + \frac{1}{2}\langle \nabla\phi_i | \mu_{\rm xc}^1 | \nabla\phi_j\rangle, \end{aligned} \quad (16)$$

and

$$\tilde{D}_{ij}^1 = \langle \phi_i| - \frac{1}{2}\nabla^2 + \tilde{v}_{\rm eff}^1 |\phi_j\rangle + \frac{1}{2}\langle \nabla\phi_i | \tilde{\mu}_{\rm xc}^1 | \nabla\phi_j\rangle. \quad (17)$$

In the above, the effective potential $v_{\rm eff}$ is the sum of the external, Hartree, and $v_{\rm xc}^{\rm GGA}$ potentials [see Eqs. (2)–(7)], and the τ-dependent-MGGA specific terms are of the form

$$\mu_{\rm eff} = -\frac{1}{2}\nabla \cdot \{\mu_{\rm xc}(\mathbf{r})\nabla\}, \quad (18)$$

where $\mu_{\rm xc}(\mathbf{r})$ is given in Eq. (8). Integration by parts has been applied to obtain the last term in Eqs. (16) and (17). The $\tilde{v}_{\rm eff}$, $\hat{D}_{ij}$, $v_{\rm eff}^1$, and $\tilde{v}_{\rm eff}^1$ are identical to those defined by Eqs. (43)–(46) of Ref. 44 [except that $v_{\rm xc}$ is replaced by the $v_{\rm xc}^{\rm GGA}$ of Eq. (7)]. Thus, compared to the usual PAW GGA Hamiltonian, three additional terms arise: $\tilde{\mu}_{\rm xc}[\tilde{n} + \hat{n} + \tilde{n}_c, \tilde{\tau} + \tilde{\tau}_c]$, $\mu_{\rm xc}^1[n^1 + n_c^1, \tau^1 + \tau_c^1]$, and $\tilde{\mu}_{\rm xc}^1[\tilde{n}^1 + \hat{n} + \tilde{n}_c^1, \tilde{\tau}^1 + \tilde{\tau}_c^1]$.

Due to the introduction of the compensation density $\hat{n}$ and the independent constructions for the partial core density $\tilde{n}_c$ and the partial core kinetic energy density $\tilde{\tau}_c$ in the PAW, the values of z could be greater than 1 in the first and third terms of Eq. (14), violating the constraint $0 \le z \le 1$[32]. For a fixed too-large spurious z, derivative discontinuity with respect

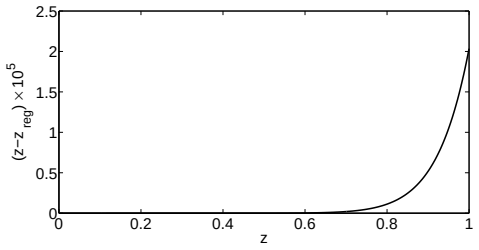

FIG. 1: The difference between z and $z_{\rm reg}$ in the range of $0 \leq z \leq 1$.

to the reduced density gradient s can be introduced into the revTPSS enhancement factor, leading to severe convergence problems. Fortunately, thanks to the facts that the formulas of revTPSS and TPSS do not have singularities for $z \geq 0$ and that the effect of the abnormal z on the total energy is canceled between the first and third terms of Eq. (14) within the augmentation spheres (exactly, if the partial wave set is complete), we can regularize z by:

$$z_{\rm reg} = \frac{z}{[1 + (z/z_{\rm inf})^m]^{1/m}}, \tag{19}$$

where we choose $z_{\rm inf} = 2$ and $m = 12$. The regularized $z_{\rm reg}$ approaches $z_{\rm inf}$ asymptotically as $z \to \infty$ and therefore removes the possibility of the discontinuity, while its effect on the exchange-correlation energy is insignificant since the difference between z and $z_{\rm reg}$ in the range of $0 \leq z \leq 1$ is negligible, as shown in Figure 1.

III. COMPUTATIONAL DETAILS

Most calculations presented in this work were performed with a developmental version of the Vienna *ab initio* simulation package (VASP), which includes the TPSS and revTPSS MGGAs. The parameters of the PAW data sets used in our calculations are summarized in Table I. These PAW files contain information about the kinetic energy density needed by the MGGA's.

In order to avoid tedious convergence tests of our results with respect to the kinetic energy cutoff of the plane wave basis set, all calculations, except for the atomization energies of the molecules in the AE6 test set, were performed at an energy cutoff of 800 eV. For calculations involving Li, we increased the energy cutoff to more than 1000 eV (1000 eV for LiCl as well as LiF and to 1200 eV for Li). The atomization energies for the AE6 molecules were calculated at an energy cutoff of 1000 eV. We determined the equilibrium lattice constants

a_0 and bulk moduli B_0 by calculating the total energy per unit cell at 7-12 points in the range $V_0 \pm 7\%$ (where V_0 is the equilibrium unit cell volume for each exchange-correlation functional), fitting the data to the stabilized jellium equation of state (SJEOS)[47–49]. The cohesive energy, defined as the energy per atom needed to atomize the crystal, is calculated for each functional from the energies of the crystal at its equilibrium volume and the spin-polarized symmetry-broken solutions of the constituent atoms (no fractional occupancies)[50]. To generate symmetry breaking, atoms and molecules were placed in a large orthorhombic box with the dimensions $10 \times 11 \times 12$ Å^3. For the Li, Na, Mg, Ca, Sr, Ba, and Rh atoms, the size of the simulation box was increased to $13 \times 14 \times 15$ Å^3. For polar molecules a dipole correction was applied, which removes the spurious interactions between repeated dipoles.

All Brillouin zone integrations for solids were performed on (16×16×16) Γ-centered symmetry reduced Monkhorst-Pack[51] k-meshes using the tetrahedron method with Blöchl correction[52]. These grids are sure to yield results that are converged with respect to the k-point sampling density. The k-point sampling for the atoms and molecules was restricted to the Γ point.

Some calculations were also performed with GAUSSIAN[53], for which a selfconsistent TPSS implementation was converted to revTPSS in Ref 7. All GAUSSIAN calculations were nonrelativistic. For the VASP calculations, the all-electron PAW partial waves are solutions of a scalar-relativistic wave equation.

As a test of our numerical implementation of the gradients, we moved along search directions $\delta\psi$ in the orbital space, comparing the direct energy change $E[\psi + \delta\psi] - E[\psi]$ to the first derivative $\langle \delta\psi | H - \epsilon S | \psi \rangle$ where $\epsilon = \langle \psi | H | \psi \rangle$ and S is the overlap matrix. Within numerical precision we found exact agreement between total energy changes and the first derivatives.

TABLE I: PAW pseudopotentials used in the present work. In the third column, the atomic orbitals treated as valence are indicated. For some elements (Li, Mg, Ca, Cu, Sr, Rh, Ag, and Ba), the local part of the pseudopotential was generated by replacing the all-electron (AE) potential of the reference atom by a soft potential (Eq. (58) of Ref[44]) within the cutoff radius $r_{\rm loc}$ (a.u.), which is provided in the "local" column. Where this radius is not shown, we show instead the lowest-energy atomic orbital that sees only the local part of the pseudopotential. Cutoff radii r_c^l (a.u.) applied for the generation of the partial waves with angular quantum number l are shown in columns 5-8, with the number N_l of valence all-electron partial-wave radial functions specified. For Si with l=0, there are two radial functions with different cutoff radii 1.5 and 1.9. $E_{\rm cut}$(eV) is the default energy cutoff of the plane wave basis set. As described in section III, we have overridden this default with higher cutoffs.

	Name	Valence	local	$N_l \times r_c^l$(a.u.)				$E_{\rm cut}$(eV)
				s	p	d	f	
Li	Li_AE_GW	1s2s	1.2	3×1.2	3×1.5	2×1.5		433
C	C_GW	2s2p	3d	2×1.2	2×1.5			414
O	O_GW	2s2p	3d	2×1.2	2×1.5			414
F	F_GW	2s2p	3d	2×1.2	2×1.5			418
Na	Na_pv_GW	2p3s	3d	2×2.2	2×2.0			259
Mg	Mg_pv_GW	2p3s	1.5	2×2.0	3×1.6			404
Al	Al_d_GW	3s3p	4f	2×1.9	2×1.9	2×1.9		241
Si	Si_d_GW	3s3p	4f	1.5 1.9	2×1.9	2×1.9		246
Cl	Cl	3s3p	3d	2×1.9	2×1.9			262
Ca	Ca_pv	3p4s	1.7	2×3.0	2×3.0	2×3.0		120
Cu	Cu_GW	3d4s	1.5	2×2.2	2×2.2	2×1.9		417
Ga	Ga_d_GW	3d4s4p	4f	2×2.0	3×2.3	3×2.0		370
Ge	Ge_d_GW	3d4s4p	4f	2×2.3	2×2.3	2×2.2		310
As	As_GW	4s4p	4f	2×2.1	2×2.1	2.1		209
Sr	Sr_sv	3s3p4s	2.2	2×2.5	2×2.5	2×2.5		226
Rh	Rh_sv_GW	4s4p4d5s	1.6	3×1.5	2×1.8	2×2.15	1 × 2.3	320
Pd	Pd_pv	4p4d5s	4f	2×2.4	2×2.1	2×2.4		251
Ag	Ag_f_GW	4d5s	1.4	2×2.5	2×2.6	2×2.4	2×2.6	250
Ba	Ba_sv	5s5p6s	2.5	2×2.8	2×2.7	2×2.7		187

IV. RESULTS AND DISCUSSIONS

A. Atomization energies of the AE6 set

The atomization energy of a molecule $D_0(M)$ is defined as the difference between the sum of the energies of the constituent atoms $\varepsilon_0(X)$ and the energy of the molecule $\varepsilon_0(M)$:

$$D_0(M) = \sum_X n_X \varepsilon_0(X) - \varepsilon_0(M), \tag{20}$$

where n_X is the number of constituent atoms X in the molecule M. Following Ref. 54, all calculations were performed using harder PAW potentials[54] instead of those given in Table I, with an energy cutoff of 1000 eV. These harder PAW's are needed[54] for accurate molecular atomization energies. The molecular geometries were taken from Ref. 55. For the analysis of the results, the following statistical quantities will be used: the mean error (ME), the mean absolute error (MAE), the mean relative error (MRE, in percent), and the mean absolute relative error (MARE, in percent).

Table II lists the atomization energies of the AE6[7,55] molecules for different functionals from VASP and GAUSSIAN. The GAUSSIAN results were calculated using the aug-cc-pV5Z(-gh) basis set, which reduced the atomization energies of $C_2H_2O_2$ by about 2 kcal/mol for PBE, TPSS, and revTPSS, compared to the smaller basis set 6-311+G(3df,2p) used for the AE6 set in Ref.[7]. Except for $C_2H_2O_2$, the basis set effects on the GAUSSIAN AE6 results are insignificant. With this larger basis set, the agreement between VASP and GAUSSIAN is excellent, with the largest difference of 1.6 kcal/mol for the revTPSS atomization energies of C_4H_8. The excellent agreement is a strong indication that the two independent implementations of revTPSS in GAUSSIAN and VASP are consistent and correct. Furthermore, it also demonstrates that the regularization of z [Eq. (19)] introduced only in VASP does not change the relative energetics. The VASP values in Table II show that PBEsol overestimates the atomization energies to an unacceptable degree (with an MAE of 34.3 kcal/mol), which is largely reduced for the PBE GGA to a reasonable value of 14.6 kcal/mol, and further reduced for the TPSS and revTPSS Meta-GGA's to 5.3 and 6.3 kcal/mol, respectively.

B. Lattice constants, bulk moduli, and cohesive energies of solids

The true force on a nucleus or the true stress on a unit cell is a derivative of the total energy with respect to a geometry parameter, and is zeroed out by minimization of the total energy with respect to geometry. By the variational principle, this force is not sensitive to small deviations of the density from full selfconsistency. The Hellmann-Feynman force on a

TABLE II: Static-nucleus atomization energies of the AE6 molecules (in kcal/mol) from the PBE and PBEsol GGA functionals, and the TPSS and revTPSS MGGAs, calculated using "harder" PAW potentials[54], instead of those given in Table I, at an energy cutoff of 1000 eV, on the standard geometries[55], as in Ref. 7. For comparison, the GAUSSIAN results using the aug-cc-pV5Z(-gh) basis set are also presented. The mean error (ME), mean absolute error (MAE), mean relative error (MRE), and mean absolute relative error (MARE) were calculated with respect to the experimental results[55], where vibrational zero-point energy[55] and spin-orbit effects[56] have been removed. V: VASP; G: GAUSSIAN. (1 kcal/mol = 0.04336 eV.)

Molecule	PBE^V	PBE^G	$PBEsol^V$	$TPSS^V$	$TPSS^G$	$revTPSS^V$	$revTPSS^G$	Expt.
SiH_4	313.2	313.5	323.2	333.7	334.0	338.1	338.6	322.8
SiO	195.8	196.3	204.6	186.9	187.0	185.7	185.9	192.7
S_2	115.4	114.9	123.9	109.8	108.6	110.3	109.0	102.8
C_3H_4	720.9	721.1	749.0	707.5	707.8	703.9	704.6	705.1
$C_2H_2O_2$	662.6	663.1	694.8	633.4	633.8	630.1	630.6	634.0
C_4H_8	1167.1	1167.7	1217.4	1154.8	1155.8	1152.5	1154.1	1149.4
ME	11.3	11.6	34.3	3.2	3.4	2.3	2.7	
MAE	14.6	14.7	34.3	5.3	5.3	6.3	6.2	
MRE(%)	3.2	3.2	8.1	1.3	1.2	1.3	1.2	
MARE(%)	4.2	4.2	8.1	2.4	2.2	2.8	2.6	

nucleus is the electrostatic force due to the charge density of electrons and other nuclei. The virial stress[57] is similarly computed from the orbitals at a single geometry. Pulay corrections arising from derivatives of the basis functions are to be included when the basis functions change with the geometry. The Hellmann-Feynman/virial values are much more sensitive to deviations from full selfconsistency than the true values are. For the small unit-cells considered here, it is practical to optimize the geometry by minimizing the energy or by zeroing out the Hellmann-Feynman forces and virial stresses. But for large unit cells the latter approach is more practical. This is the reason why full selfconsistency is important. In order to test that the virial stress tensor is correctly implemented for MGGA's, we used it to calculate the lattice constants for three solids (Al, C, and MgO) . Table III shows that the lattice constants obtained this way agree very closely with those found by fitting the energy

TABLE III: PBE, TPSS, and revTPSS lattice constants a_0 (in Å) of Al, C, and MgO obtained by fitting the energy-volume data to the stabilized jellium equation of state (EOS), and by relaxing (REL) the unit cell size and shape to zero out the virial stresses.

	EOS_PBE	REL_PBE	EOS_revTPSS	REL_revTPSS	EOS_TPSS	REL_TPSS
Al	4.035	4.034	4.005	4.005	4.008	4.007
C	3.569	3.569	3.558	3.558	3.568	3.567
MgO	4.261	4.260	4.240	4.237	4.244	4.241

to an equation of state (EOS), for the PBE, TPSS, and revTPSS functionals. Similarly, the bond lengths of selected diatomic molecules, found by zeroing out the Hellmann-Feynman forces on the nuclei, were the same as those found by total energy minimization. These tests confirm that the selfconsistency of MGGA's has been implemented successfully.

In the rest of this work, we will compute lattice constants by minimizing the total energy (fitted to an equation of state[47–49]) with respect to the lattice constant. We will use selfconsistent densities, although the effect of using say the LSDA density instead of the selfconsistent one would be small[58]. Tables IV, V and VI give the lattice constants, bulk moduli and cohesive energies obtained using the LSDA, GGAs (PBE, PBEsol, and AM05), and MGGAs (TPSS and revTPSS) for a set of 20 cubic solids. The experimental lattice constants have been corrected to static-lattice values by subtracting the zero-point anharmonic expansion (ZPAE)[7,38], and the experimental bulk moduli presented in Table V have been corrected for the zero-point phonon effects (ZPPE)[38,58]. We have used the calculated full quasiharmonic phonon spectrum wherever it was available from Ref.[38]. Full phonon-spectrum estimates for about 60 solids will be available soon[59]. The experimental cohesive energies were corrected for the zero-point vibration energy[38,47].

As usual, the LSDA functional underestimates the lattice constants while PBE overestimates them by roughly the same amount in terms of MAE. revTPSS, among all the considered functionals, delivers the best lattice constants on average with an MAE of 0.032 Å. This is slightly better than the performance of PBEsol and AM05, the GGAs designed for solids. TPSS predicts slightly too long lattice constants with an MAE of 0.043 Å, though still better than those of PBE.

For the elements of group IA (Li and Na) and group IIA (Ca, Sr, and Ba), revTPSS

corrects the underestimations of LSDA and PBEsol, and yields lattice constants of similar quality as PBE and TPSS. The lattice constant of Al does not seem to be very sensitive to the choice of exchange-correlation functionals. LSDA yields the largest absolute error (0.035 Å) for Al, while for all other functionals the absolute error is <0.02 Å. For the elements of group IVA with diamond structure (C, Si, and Ge), the trend previously found for LSDA, GGAs, and the TPSS MGGA (see Refs.[38,60]) applies to the revTPSS as well: The overestimation of the revTPSS lattice constants with respect to experiment increases with the nuclear charge Z, from 0.005 Å for C, to 0.018 Å for Si, and then to 0.038 Å for Ge. For the lattice constants of the transition-metal elements, revTPSS is comparable to PBEsol. It yields good equilibrium lattice constants for 4d and 5d elements with absolute relative errors smaller than 0.5%, but underestimates the lattice constant for the 3d elemental metal Cu (with an absolute relative error of 1.0%). For the series of IA-VIIA and IIA-VIA compounds (LiF, LiCl, NaF, NaCl, and MgO), revTPSS performs slightly better than TPSS, but still overestimates the lattice constants, by up to 2.1% (for NaF). As observed earlier, the AM05 functional gives too long lattice constants for some of these ionic solids, similar to TPSS and revTPSS, while PBEsol gives reasonable estimates[58].

Errors in the theoretical lattice constant with respect to experiment translate into comparatively large discrepancies in the bulk moduli B_0. (The calculated bulk moduli are quite sensitive to the equilbrium volume). As usual an underestimation of the lattice constants shows a one-to-one correlation with an overestimation of the bulk moduli. Thus LSDA overestimates the bulk moduli while PBE underestimates them (see Table V). revTPSS yields the MAE of 8.664 GPa, slightly larger than 7.942 GPa, the MAE of TPSS. Among all the considered functionals, PBEsol gives the smallest MARE, 5.69%. Note, however, that the individual bulk moduli have experimental uncertainties up to 5 or 10 %[58].

Table VI shows that LSDA strongly overestimates the cohesive energies. The PBE cohesive energies are underestimated with respect to experiment, but with a reasonable MAE, 0.144 eV. PBEsol, as expected, overestimates the cohesive energies with a MAE of 0.253 eV, i.e., between those of LSDA and PBE. The experimental uncertainty is up to 0.08 eV (Si)[58]. revTPSS underestimates the cohesive energies for all the insulators and semiconductors considered here, while overestimating for all the metals except Li. Unfortunately, the revTPSS and TPSS do not improve, but actually worsen the cohesive energies compared to PBE. This is not what one might expect considering the performance of these MGGAs for

the atomization energies of the molecules in the AE6 set.

For a given functional, there is generally good agreement between our PAW results and the full potential linearized augmented plane wave (FLAPW) results of Ref.[60], as expected[54] for carefully converged calculations.

C. Magnetic moment of solids Fe and Ni

It is well known that the PBE GGA corrects a qualitatively wrong prediction of LSDA for the solid phase of Fe. LSDA predicts for Fe that the ground state is nonmagnetic face-centered-cubic instead of the experimentally-observed ferromagnetic body-centered-cubic[62,63]. Table VII shows that both TPSS and revTPSS have lower total energies at each equilibrium lattice constant for bcc Fe than for fcc Fe, and therefore predict the right ground state. Furthermore, the magnetic moments of TPSS and revTPSS for bcc Fe and fcc Ni are close to the PBE values and in good agreement with the experimental results. However, Table VII also shows that the lattice constants from TPSS and revTPSS are too short while the bulk moduli are too large compared to the experimental results.

In our Table VII, we have also included PBEsol GGA results. We find that PBEsol correctly makes the magnetic bcc phase of Fe more stable than the nonmagnetic fcc phase. However, Söderlind and Gonis[66] found that it incorrectly makes the nonmagnetic hcp phase very slightly more stable than the magnetic bcc phase, by about 0.01 eV/atom.

V. CONCLUSIONS

In this work, the TPSS and revTPSS MGGAs were implemented self-consistently within the framework of the PAW method using a plane wave basis set. We assessed the performance of TPSS and revTPSS MGGAs for the prediction of structural properties of solids (equilibrium lattice constants, bulk moduli), and thermochemical properties of solids and molecules

(cohesive energies, atomization energies). For this purpose, the AE6 set of molecules and a representative test set of 20 materials comprising ionic, semiconducting, and metallic systems were chosen.

By restoring the second-order gradient expansion for exchange over a wide range of densities as the PBEsol[19] GGA did, and by respecting the paradigms of both condensed matter physics and quantum chemistry as the TPSS[6] did, revTPSS[7] predicts lattice constants and bulk moduli for the 20 solids as good as PBEsol and atomization energies for the molecules of the AE6 set comparable to TPSS. However, unexpectedly, revTPSS (and TPSS) only slightly improve the cohesive energies over PBEsol for our 20 solids on average, and are less accurate than PBE for this property. Another interesting observation is that revTPSS underestimates the cohesive energies for all the insulators and semiconductors considered here while overestimating for all the metals except Li. The errors of revTPSS (and PBEsol) cohesive energies and bulk moduli are especially large for the transition metals Cu, Rh, and Pd (but not Ag), where PBE typically works better. Both TPSS and revTPSS predict the correct ground-state solid phase for Fe, the ferromagnetic body-centered-cubic (bcc) structure, with an accurate magnetic moment.

Neither our meta-GGA cohesive energies nor our conclusions about them are the same as those of Ref. 7. The revTPSS cohesive energies of Ref. 7 were computed for the metals by the all-electron code BAND, and for the insulators by a mix of BAND and older nonselfconsistent VASP calculations. Some of the BAND cohesive energies of Ref. 7 were not converged, and the VASP cohesive energies of Ref. 7 were based on an older and less-complete implementation of revTPSS. In particular, the revTPSS cohesive energies reported in Ref. 7 were too high for Al, SiC, Si, Ge, LiCl, NaCl, and MgO.

The exact density functional for the exchange-correlation energy is of course fully nonlocal, and fully-nonlocal approximations are known to be needed in certain situations (long-range van der Waals attraction, and sharing of electrons over stretched bonds). But semilocal functionals are more computationally efficient. The highest-level semilocal functional, the meta-GGA, has the potential to treat correctly effects that cannot be so treated in LSDA or GGA, and probably has sufficient complexity to permit further refinement beyond the revTPSS form.

Acknowledgments

This work was partially supported by the IMI Program of the National Science Foundation under Award No. DMR04-09848. Portions of this research were conducted with high performance computational resources provided by the Louisiana Optical Network Initiative (http://www.loni.org/). JS, GIC, AR, PH, and JPP acknowledge NSF support under Grant No. DMR-0854769. Three of us (MM, YSK, and GK) were supported by the Austrian *Fonds zur Förderung der wissenschaftlichen Forschung (FWF)*. GIC thanks the support by the New Hungary Development Plan (Project ID: TAMOP-4.2.1/B-09/1/KMR-2010-0002) for the scientific program of the "Development of quality-oriented and harmonized R+D+I strategy and functional model at BME" project.

Appendix A: TPSS and revTPSS meta-GGAs for exchange

Although TPSS and revTPSS have been implemented selfconsistently in several codes, the required derivatives (Appendices A and B) have not been published until now. The revTPSS exchange functional for a spin-unpolarized system can be written as:

$$E_x^{\mathrm{revTPSS}}[n] = \int d^3r e_x^{\mathrm{revTPSS}} = \int d^3r e_x^{\mathrm{LDA}} F_x^{\mathrm{revTPSS}}(p,z), \tag{A1}$$

where e_x^{revTPSS} is the exchange energy density of revTPSS and $e_x^{\mathrm{LDA}} = -(3/4\pi)(3\pi^2)^{1/3}n^{4/3}$ is the exchange energy density of a uniform electron gas at density n. The two dimensionless inhomogeneity parameters are

$$p = |\nabla n|^2/[4(3\pi^2)^{2/3}n^{8/3}] = s^2, \tag{A2}$$

the square of the reduced gradient s, and

$$z = \tau^W/\tau, \tag{A3}$$

where

$$\tau^W = |\nabla n|^2/8n, \tag{A4}$$

is the von Weizsäcker kinetic energy density and $\tau = \sum_\sigma \tau_\sigma$. Here the kinetic energy density of electrons with spin σ ($\sigma = \uparrow, \downarrow$) is defined, in terms of the occupied Kohn-Sham orbitals $\psi_{\mathrm{k}\sigma}(r)$, as

$$\tau_\sigma(r) = \sum_k^{\mathrm{occup}} \frac{1}{2}|\nabla\psi_{\mathrm{k}\sigma}(r)|^2. \tag{A5}$$

The revTPSS enhancement factor for exchange is:

$$F_x^{\rm revTPSS}(p,z) = 1 + \kappa - \kappa/(1 + x/\kappa), \tag{A6}$$

with

$$x = (s_1 + s_2 + s_3 + s_4 + s_5 + s_6)/s_7, \tag{A7}$$

where $s_1 = [\frac{10}{81} + \frac{cz^3}{(1+z^2)^2}]p$, $s_2 = \frac{146}{2025}\tilde{q}_b^2$, $s_3 = -\frac{73}{405}\tilde{q}_b\sqrt{\frac{1}{2}(\frac{3}{5}\mathrm{z})^2 + \frac{1}{2}\mathrm{p}^2}$, $s_4 = \frac{1}{\kappa}(\frac{10}{81})^2 p^2$, $s_5 = 2\sqrt{e}\frac{10}{81}(\frac{3}{5}z)^2$, $s_6 = e\mu p^3$, and $s_7 = (1 + \sqrt{e}p)^2$. Here $\tilde{q}_b = \frac{9}{20}(\alpha - 1)/[1 + b\alpha(\alpha - 1)]^{1/2} + \frac{2}{3}p$ with $\alpha = \frac{\tau - \tau^W}{\tau^{\rm unif}} = \frac{5}{3}p(z^{-1} - 1)$, where $\tau^{\rm unif} = \frac{3}{10}(3\pi^2)^{2/3}n^{5/3}$ is the Thomas-Fermi kinetic energy density. In revTPSS, $\kappa = 0.804$, $c = 2.35204$, $e = 2.1677$, $b = 0.4$, and $\mu = 0.14$.

Let y stand for $n, |\nabla n|$, or τ. The derivatives of $F_x^{\rm revTPSS}$ with respect to y can be written as:

$$\frac{\partial F_x^{\rm revTPSS}}{\partial y} = (1 + x/\kappa)^{-2}\frac{\partial x}{\partial y}, \tag{A8}$$

where

$$\frac{\partial x}{\partial y} = \frac{1}{s_7}(\frac{\partial s_1}{\partial y} + \frac{\partial s_2}{\partial y} + \frac{\partial s_3}{\partial y} + \frac{\partial s_4}{\partial y} + \frac{\partial s_5}{\partial y} + \frac{\partial s_6}{\partial y}) - \frac{x}{s_7}\frac{\partial s_7}{\partial y}, \tag{A9}$$

$$\frac{\partial s_1}{\partial y} = \frac{cpz^2(3 - z^2)}{(1 + z^2)^3}\frac{\partial z}{\partial y} + [\frac{10}{81} + \frac{cz^3}{(1 + z^2)^2}]\frac{\partial p}{\partial y}, \tag{A10}$$

$$\frac{\partial s_2}{\partial y} = \frac{292}{2025}\tilde{q}_b\frac{\partial \tilde{q}_b}{\partial y}, \tag{A11}$$

$$\frac{\partial s_3}{\partial y} = -\frac{73}{405}\{\sqrt{\frac{1}{2}(\frac{3}{5}\mathrm{z})^2 + \frac{1}{2}\mathrm{p}^2}\frac{\partial \tilde{q}_b}{\partial y} + \frac{\tilde{q}_b(\frac{9}{25}z\frac{\partial z}{\partial y} + p\frac{\partial p}{\partial y})}{2\sqrt{\frac{1}{2}(\frac{3}{5}\mathrm{z})^2 + \frac{1}{2}\mathrm{p}^2}}\}, \tag{A12}$$

$$\frac{\partial s_4}{\partial y} = \frac{2}{\kappa}(\frac{10}{81})^2 p\frac{\partial p}{\partial y}, \tag{A13}$$

$$\frac{\partial s_5}{\partial y} = 4\sqrt{e}\frac{10}{81}(\frac{3}{5})^2 z\frac{\partial z}{\partial y}, \tag{A14}$$

$$\frac{\partial s_6}{\partial y} = 3e\mu p^2\frac{\partial p}{\partial y}, \tag{A15}$$

$$\frac{\partial s_7}{\partial y} = 2\sqrt{e}(1 + \sqrt{e}p)\frac{\partial p}{\partial y}, \tag{A16}$$

and

$$\frac{\partial \tilde{q}_b}{\partial y} = \frac{3}{4}\frac{1 + (\alpha - 1)b/2}{[1 + b\alpha(\alpha - 1)]^{3/2}}[(z^{-1} - 1)\frac{\partial p}{\partial y} - \frac{p}{z^2}\frac{\partial z}{\partial y}] + \frac{2}{3}\frac{\partial p}{\partial y}. \tag{A17}$$

Here $\frac{\partial p}{\partial n} = -\frac{8}{3}n^{-1}p$, $\frac{\partial p}{\partial |\nabla n|} = \frac{2p}{|\nabla n|}$, $\frac{\partial p}{\partial \tau} = 0$, $\frac{\partial z}{\partial n} = -z/n$, $\frac{\partial z}{\partial |\nabla n|} = \frac{2z}{|\nabla n|}$, and $\frac{\partial z}{\partial \tau} = -z/\tau$.

Therefore,

$$\frac{\partial e_x^{\rm revTPSS}}{\partial n} = v_x^{\rm LDA} F_x^{\rm revTPSS} + e_x^{\rm LDA} \frac{\partial F_x^{\rm revTPSS}}{\partial n}, \tag{A18}$$

$$\frac{\partial e_x^{\rm revTPSS}}{\partial \nabla n} = e_x^{\rm LDA} \frac{\partial F_x^{\rm revTPSS}}{\partial |\nabla n|} \frac{\nabla n}{|\nabla n|}, \tag{A19}$$

and

$$\frac{\partial e_x^{\rm revTPSS}}{\partial \tau} = e_x^{\rm LDA} \frac{\partial F_x^{\rm revTPSS}}{\partial \tau}, \tag{A20}$$

where $v_x^{\rm LDA} = -\frac{1}{\pi}(3\pi^2 n)^{1/3}$.

The exchange energy for a spin-polarized system may be evaluated from the exchange functional for a spin-unpolarized system using the spin-scaling relation[67],

$$E_x[n_\uparrow, n_\downarrow] = E_x[2n_\uparrow]/2 + E_x[2n_\downarrow]/2. \tag{A21}$$

And the derivatives of the exchange energy density of the spin-polarized system with respect to $n_\sigma, |\nabla n_\sigma|$,and τ_σ can be obtained accordingly.

Compared to revTPSS, the differences of TPSS for exchange are in s_1 with $s_1 = [\frac{10}{81} + \frac{cz^2}{(1+z^2)^2}]p$ and $\frac{\partial s_1}{\partial y} = \frac{2cpz(1-z^2)}{(1+z^2)^3}\frac{\partial z}{\partial y} + [\frac{10}{81} + \frac{cz^2}{(1+z^2)^2}]\frac{\partial p}{\partial y}$ as well as in the parameters ($c = 1.59096$, $e = 1.537$, and $\mu = 0.21951$).

Appendix B: TPSS and revTPSS meta-GGAs for correlation

The revTPSS correlation functional for a spin-polarized system can be written as:

$$E_c^{\rm revTPSS}[n_\uparrow, n_\downarrow] = \int d^3r e_c^{\rm revTPSS} = \int d^3r n \epsilon_c^{\rm revPKZB}[1 + d\epsilon_c^{\rm revPKZB} z^3], \tag{B1}$$

where

$$\epsilon_c^{\rm revPKZB} = \epsilon_c^{\widetilde{\rm PBE}}[1 + C(\zeta,\xi)z^2] - [1 + C(\zeta,\xi)]z^2\epsilon_c^{\rm ave}, \tag{B2}$$

$$\epsilon_c^{\rm ave} = \sum_\sigma \frac{n_\sigma}{n}\tilde{\epsilon}_c^\sigma, \tag{B3}$$

and

$$\tilde{\epsilon}_c^\sigma = max[\epsilon_c^{\widetilde{\rm PBE}}(n_\sigma, 0, \nabla n_\sigma, 0), \epsilon_c^{\widetilde{\rm PBE}}(n_\uparrow, n_\downarrow, \nabla n_\uparrow, \nabla n_\downarrow)]. \tag{B4}$$

$\epsilon_c^{\widetilde{\rm PBE}}$ is the PBE correlation energy per electron but with the second-order gradient expansion coefficient in its expression made r_s-dependent[7,68], $\beta(r_s) = 0.0066725(1 + 0.1r_s)/(1 + 0.1778r_s)$, where the seitz radius is $r_s = (3/4\pi n)^{1/3}$. Its derivatives with respect to n_σ and $|\nabla n_\sigma|$ can be written as $\frac{\partial \epsilon_c^{\widetilde{\rm PBE}}}{\partial n_\sigma} = \frac{\partial \epsilon_c^{\rm PBE}}{\partial n_\sigma}|_{\beta=\beta({\rm r_s})} + \frac{\partial \epsilon_c^{\rm PBE}}{\partial \beta}|_{\beta=\beta({\rm r_s})}\frac{\partial \beta(r_s)}{\partial r_s}\frac{\partial r_s}{\partial n_\sigma}$ and $\frac{\partial \epsilon_c^{\widetilde{\rm PBE}}}{\partial |\nabla n_\sigma|} =$

$\frac{\partial \epsilon_c^{\rm PBE}}{\partial |\nabla n_\sigma|}|_{\beta=\beta(r_s)}$, where $\frac{\partial \beta(r_s)}{\partial r_s} = \frac{-0.0778\times 0.0066725}{(1+0.1778 r_s)^2}$ and $\frac{\partial r_s}{\partial n_\sigma} = -r_s/3n$. The function $C(\zeta,\xi)$ has the expression,

$$C(\zeta,\xi) = \frac{c_1 + c_2\zeta^2 + c_3\zeta^4 + c_4\zeta^6}{\{1+\xi^2[(1+\zeta)^{-4/3}+(1-\zeta)^{-4/3}]/2\}^4}, \tag{B5}$$

where the spin-polarization $\zeta = \frac{n_\uparrow - n_\downarrow}{n_\uparrow + n_\downarrow}$, and $\xi = \frac{|\nabla\zeta|}{2(3\pi^2 n)^{1/3}}$. Here $d = 2.8$, $c_1 = 0.59$, $c_2 = 0.9269$, $c_3 = 0.6225$, and $c_4 = 2.1540$.

Let y stand for $n_\sigma, |\nabla n_\sigma|$, or τ_σ. The derivatives of $\epsilon_c^{\rm revPKZB}$ with respect to y can be written as:

$$\begin{aligned}\frac{\partial \epsilon_c^{\rm revPKZB}}{\partial y} &= [1+C(\zeta,\xi)z^2]\frac{\partial \widetilde{\epsilon_c^{\rm PBE}}}{\partial y} - z^2[1+C(\zeta,\xi)]\frac{\partial \epsilon_c^{\rm ave}}{\partial y} + z^2(\widetilde{\epsilon_c^{\rm PBE}} - \epsilon_c^{\rm ave})\frac{\partial C(\zeta,\xi)}{\partial y} + \\ &\quad +2z\{C(\zeta,\xi)\widetilde{\epsilon_c^{\rm PBE}} - [1+C(\zeta,\xi)]\epsilon_c^{\rm ave}\}\frac{\partial z}{\partial y},\end{aligned} \tag{B6}$$

where

$$\begin{aligned}\frac{\partial C(\zeta,\xi)}{\partial y} &= \{\frac{2c_2\zeta + 4c_3\zeta^3 + 6c_4\zeta^5}{c_1 + c_2\zeta^2 + c_3\zeta^4 + c_4\zeta^6} + \frac{8\xi^2[(1+\zeta)^{-7/3} - (1-\zeta)^{-7/3}]/3}{1+\xi^2[(1+\zeta)^{-4/3}+(1-\zeta)^{-4/3}]/2}\}C(\zeta,\xi)\frac{\partial\zeta}{\partial y} - \\ &\quad -\frac{4\xi[(1+\zeta)^{-4/3}+(1-\zeta)^{-4/3}]}{1+\xi^2[(1+\zeta)^{-4/3}+(1-\zeta)^{-4/3}]/2}C(\zeta,\xi)\frac{\partial\xi}{\partial y}.\end{aligned} \tag{B7}$$

For $\epsilon_c^{\rm ave}$, we have

$$\frac{\partial \epsilon_c^{\rm ave}}{\partial n_\sigma} = \sum_\eta (\frac{\delta_{\eta\sigma} n - n_\eta}{n^2}\tilde{\epsilon}_c^\eta + \frac{n_\eta}{n}\frac{\partial \tilde{\epsilon}_c^\eta}{\partial n_\sigma}), \tag{B8}$$

$$\frac{\partial \epsilon_c^{\rm ave}}{\partial |\nabla n_\sigma|} = \sum_\eta \frac{n_\eta}{n}\frac{\partial \tilde{\epsilon}_c^\eta}{\partial |\nabla n_\sigma|}. \tag{B9}$$

and

$$\frac{\partial \epsilon_c^{\rm ave}}{\partial \tau} = 0, \tag{B10}$$

with $\frac{\partial \tilde{\epsilon}_c^\eta}{\partial y} = \frac{\partial \widetilde{\epsilon_c^{\rm PBE}}(n_\eta,0,\nabla n_\eta,0)}{\partial y}\delta_{\eta\sigma}$ if $\widetilde{\epsilon_c^{\rm PBE}}(n_\eta,0,\nabla n_\eta,0) > \widetilde{\epsilon_c^{\rm PBE}}(n_\uparrow,n_\downarrow,\nabla n_\uparrow,\nabla n_\downarrow)$ and $\frac{\partial \tilde{\epsilon}_c^\eta}{\partial y} = \frac{\partial \widetilde{\epsilon_c^{\rm PBE}}(n_\uparrow,n_\downarrow,\nabla n_\uparrow,\nabla n_\downarrow)}{\partial y}$ if $\widetilde{\epsilon_c^{\rm PBE}}(n_\eta,0,\nabla n_\eta,0) < \widetilde{\epsilon_c^{\rm PBE}}(n_\uparrow,n_\downarrow,\nabla n_\uparrow,\nabla n_\downarrow)$. Here $\frac{\partial\zeta}{\partial n_\sigma} = \frac{\delta_{\sigma\uparrow}-\delta_{\sigma\downarrow}-\zeta}{n}$, $\frac{\partial\zeta}{\partial|\nabla n_\sigma|} = \frac{\partial\zeta}{\partial\tau} = 0$, $\frac{\partial z}{\partial n_\sigma} = -z/n$, $\frac{\partial z}{\partial|\nabla n_\sigma|} = \frac{1}{4n\tau}[|\nabla n_\sigma| + \frac{\nabla n_\uparrow\cdot\nabla n_\downarrow}{|\nabla n_\sigma|}]$, $\frac{\partial z}{\partial\tau_\sigma} = -z/\tau$, $\frac{\partial\xi}{\partial n_\sigma} = \frac{1}{2(3\pi^2 n)^{1/3}}\{-\frac{7}{3}\frac{|\nabla\zeta|}{n} + \frac{4[n_\downarrow|\nabla n_\uparrow|^2\delta_{\sigma\downarrow} - \nabla n_\uparrow\cdot\nabla n_\downarrow(n_\uparrow\delta_{\sigma\downarrow}+n_\downarrow\delta_{\sigma\uparrow}) + n_\uparrow|\nabla n_\downarrow|^2\delta_{\sigma\uparrow}]}{n^4|\nabla\zeta|}\}$, $\frac{\partial\xi}{\partial\tau} = 0$, $\frac{\partial\xi}{\partial|\nabla n_\sigma|} = \frac{2n_\downarrow^2|\nabla n_\uparrow|\delta_{\sigma\uparrow} + 2n_\uparrow^2|\nabla n_\downarrow|\delta_{\sigma\downarrow} - 2n_\uparrow n_\downarrow\nabla n_\uparrow\cdot\nabla n_\downarrow/|\nabla n_\sigma|}{(3\pi^2 n)^{1/3}n^4|\nabla\zeta|}$, and $|\nabla\zeta| = 2[n_\downarrow^2|\nabla n_\uparrow|^2 - 2n_\uparrow n_\downarrow\nabla n_\uparrow\cdot\nabla n_\downarrow + n_\uparrow^2|\nabla n_\downarrow|^2]^{1/2}/n^2$.

Therefore,

$$\begin{aligned}\frac{\partial e_c^{\rm revTPSS}}{\partial n_\sigma} &= dn\epsilon_c^{\rm revPKZB}[z^3\frac{\partial \epsilon_c^{\rm revPKZB}}{\partial n_\sigma} + 3z^2\epsilon_c^{\rm revPKZB}\frac{\partial z}{\partial n_\sigma}] + \\ &\quad +(\epsilon_c^{\rm revPKZB} + n\frac{\partial \epsilon_c^{\rm revPKZB}}{\partial n_\sigma})[1+d\epsilon_c^{\rm revPKZB}z^3],\end{aligned} \tag{B11}$$

$$\frac{\partial e_c^{\rm revTPSS}}{\partial \nabla n_\sigma} = \{dn\epsilon_c^{\rm revPKZB}[z^3\frac{\partial \epsilon_c^{\rm revPKZB}}{\partial|\nabla n_\sigma|} + 3z^2\epsilon_c^{\rm revPKZB}\frac{\partial z}{\partial|\nabla n_\sigma|}] + +n\frac{\partial \epsilon_c^{\rm revPKZB}}{\partial|\nabla n_\sigma|}[1 + d\epsilon_c^{\rm revPKZB}z^3]\}\frac{\nabla n}{|\nabla n|}, \quad \text{(B12)}$$

and

$$\frac{\partial e_c^{\rm revTPSS}}{\partial \tau_\sigma} = dn\epsilon_c^{\rm revPKZB}[z^3\frac{\partial \epsilon_c^{\rm revPKZB}}{\partial \tau_\sigma} + 3z^2\epsilon_c^{\rm revPKZB}\frac{\partial z}{\partial \tau_\sigma}] + +n\frac{\partial \epsilon_c^{\rm revPKZB}}{\partial \tau_\sigma}[1 + d\epsilon_c^{\rm revPKZB}z^3]. \quad \text{(B13)}$$

TPSS has the same formula for correlation as revTPSS, but uses the original PBE correlation energy per electron, where $\beta = 0.0066725$ is r_s-independent. The parameters in $C(\zeta, \xi)$ used in TPSS are $c_1 = 0.53$, $c_2 = 0.87$, $c_3 = 0.50$, and $c_4 = 2.26$.

---

[1] W. Kohn and L.J. Sham, Phys. Rev. **140**, A1133 (1965).

[2] R.G. Parr and W. Yang, *Density Functional Theory of Atoms and Molecules* (Oxford University Press, Oxford, 1989).

[3] J.P. Perdew and S. Kurth, *A Primer in Density Functional Theory* (Springer Lecture Notes in Physics, Vol. **620**, 2003).

[4] J.P. Perdew and Y. Wang, Phys. Rev. B **45**, 13244 (1992).

[5] J.P. Perdew, K. Burke, and M. Ernzerhof, Phys. Rev. Lett. **77**, 3865 (1996).

[6] J. Tao, J.P. Perdew, V.N. Staroverov, and G.E. Scuseria, Phys. Rev. Lett. **91**, 146401 (2003).

[7] J.P. Perdew, A. Ruzsinszky, G.I. Csonka, L.A. Constantin, and J. Sun, Phys. Rev. Lett. **103**, 026403 (2009); *ibid.* **106**, 179902 (2011) (E).

[8] J. P. Perdew and K. Schmidt, in *Density Functional Theory and Its Applications to Materials*, edited by V. E. van Doren, C. van Alsenoy, and P. Geerlings (American Institute of Physics, 2001).

[9] G.I. Csonka, O.A. Vydrov, G.E. Scuseria, A. Ruzsinszky, and J.P. Perdew, J. Chem. Phys. **126**, 244107 (2007).

[10] J.P. Perdew, Phys. Rev. B **33**, 8822 (1986).

[11] J.P. Perdew, K. Burke, and Y. Wang, Phys. Rev. B **54**, 16533 (1996).

[12] J.P. Perdew and Y. Wang, Phys. Rev. B **33**, 8800 (1986).

[13] D.C. Langreth and M.J. Mehl, Phys. Rev. B **28**, 1809 (1983).

[14] C. Lee, W. Yang, and R.G. Parr, Phys. Rev. B **37**, 785 (1988).

[15] B. Hammer, L.B. Hansen, and J.K. Norskov, Phys. Rev. B **59**, 7413 (1999).

[16] A.D. Becke, Phys. Rev. A **38**, 3098 (1988).

[17] A.D. Becke, J. Chem. Phys. **88**, 1053 (1988).

[18] R. Armiento and A.E. Mattsson, Phys. Rev. B **72**, 085108 (2005).

[19] J.P. Perdew, A. Ruzsinszky, G.I. Csonka, O.A. Vydrov, G.E. Scuseria, L.A. Constantin, X. Zhou, and K. Burke, Phys. Rev. Lett. **100**, 136406 (2008).

[20] E. Engel and S.H. Vosko, Phys. Rev. B **50**, 10498 (1994).

[21] M. Filatov and W. Thiel, Phys. Rev. A **57**, 189 (1998).

[22] E.I. Proynov, A. Vela, E. Ruiz, and D.R. Salahub, Int. J. Quantum Chem. Symp. **29**, 61 (1995).

[23] T. van Voorhis and G.E. Scuseria, J. Chem. Phys. **109**, 400 (1998).

[24] M. Ernzerhof and G.E. Scuseria, J. Chem. Phys. **111**, 911 (1999).

[25] J.P. Perdew, S. Kurth, A. Zupan, and P. Blaha, Phys. Rev. Lett. **82**, 2544 (1999).

[26] Y. Zhao and D.G. Truhlar, J. Chem. Phys. **125**, 194101 (2006).

[27] Y. Zhao and D.G. Truhlar, J. Chem. Phys. **128**, 184109 (2008).

[28] A.D. Becke and M.R. Roussel, Phys. Rev. A **39**, 3761 (1989).

[29] A.D. Becke, J. Comput. Chem. **20**, 63 (1999).

[30] A.D. Becke, Int. J. Quantum Chem. **23**, 1915 (1983).

[31] A.D. Becke, J. Chem. Phys. **109**, 2092 (1998).

[32] S. Kurth, J.P. Perdew, and P. Blaha, Int. J. Quantum Chem. **75**, 889 (1999).

[33] V.N. Staroverov, G.E. Scuseria, J. Tao, and J.P. Perdew, J. Chem. Phys. **119**, 12129 (2003).

[34] F. Furche and J.P. Perdew, J. Chem. Phys. **124**, 044103 (2006).

[35] J. Enkovaara, C. Rostgaard, J.J. Mortensen, J. Chen, M. Dulak, L. Ferrighi, J. Gavnholt, C. Glinsvad, V. Haikola, H.A. Hansen, H.H. Kristoffersen, M. Kuisma, A.H. Larsen, L. Lehtovaara, M. Ljungberg, O. Lopez-Acevedo, P.G. Moses, J. Ojanen, T. Olsen, V. Petzold, N.A. Romero, J. Stausholm-Møller, M. Strange, G.A. Tritsaris, M. Vanin, M. Walther, B. Hammer, H. Häkkinen, G.K.H. Madsen, R.M. Nieminen, J.K. Nørskov, M. Puska, T.T. Rantala, J. Schiøtz, K.S. Thygesen, and K.W. Jacobsen, J. Phys.: Condensed Matter. **22**, 253202 (2010).

[36] J. Sun, M. Marsman, A. Ruzsinszky, G. Kresse, and J.P. Perdew, Phys. Rev. B (Rapid Communication) **83**,121410 (2011).

[37] G.I. Csonka, J.P. Perdew, and A. Ruzsinszky, J. Chem. Theor. Comput. **6**, 3688 (2010).

[38] L. Schimka, J. Harl, and G. Kresse, J. Chem. Phys **134**, 024116 (2011).

[39] A.V. Arbuznikov and M. Kaupp, Chemical Physics Letters **381**, 495 (2003).

[40] R.T. Sharp and G. Horton, Phys. Rev. **90**, 317 (1953).

[41] J.D. Talman and W. Shadwick, Phys. Rev. A **14**, 36 (1976).

[42] R. Neumann, R.H. Nobes, and N.C. Handy, Mol. Phys. **87**, 1 (1996).

[43] P.E. Blöchl, Phys. Rev. B **50**, 17953 (1994).

[44] G. Kresse and D. Joubert, Phys. Rev. B **59**, 1758 (1999).

[45] A.E. Mattsson, R. Armiento R, J. Paier, G. Kresse, J.M. Wills, and T.R. Mattsson, J. Chem. Phys **128**, 084714-1–11 (2008).

[46] P.E. Blöchl, C.J. Först, and J. Schimpl, Bull. Mater. Sci, **26**, 33 (2003).

[47] A.B. Alchagirov, J.P. Perdew, J.C. Boettger, R.C. Albers, and C. Fiolhais, Phys. Rev. B **63**, 224115 (2001).

[48] A.B. Alchagirov, J.P. Perdew, J.C. Boettger, R.C. Albers, and C. Fiolhais, Phys. Rev. B **67**, 026103 (2003).

[49] V.N. Staroverov, G.E. Scuseria, J. Tao, and J.P. Perdew, Phys. Rev. B **69**, 075102 (2004).

[50] F.W. Kutzler and G.S. Painter, Phys. Rev. Lett. **59**, 1285 (1987).

[51] H.J. Monkhorst and J. Pack, Phys. Rev. B **13**, 5188 (1976).

[52] P.E. Blöchl, O. Jepsen, and O.K. Andersen, Phys. Rev. B **49**, 16223 (1994).

[53] M.J. Frisch, G.W. Trucks, H.B. Schlegel, G.E. Scuseria, *et. al.*, Gaussian, Inc., Wallingford CT, 2004.

[54] J. Paier, M. Marsman, K. Hummer, G. Kresse, I.C. Gerber, and J.G. Angyan, J. Chem. Phys. **124**, 154709 (2006).

[55] B.J. Lynch and D.G. Truhlar, Journal of Physical Chemistry A **107**, 8996 (2003).

[56] B.J. Lynch, D.G. Truhlar, Journal of Physical Chemistry A, *submitted*; http://t1.chem.umn.edu/misc/database_group/database_therm_bh/ae6bh6.pl.

[57] O.H. Nielsen and R.M. Martin, Phys. Rev. Lett. 50, 697 (1983).

[58] G.I. Csonka, J.P. Perdew, A. Ruzsinszky, P.H.T. Philipsen, S. Lebegue, J. Paier, O.A. Vydrov, and J.G. Angyan, Phys. Rev. B **79**, 155107 (2009).

[59] P. Hao, Y. Fang, P.H.T. Philipsen, J. Sun, and J.P. Perdew, unpublished.

[60] P. Haas, F. Tran, and P. Blaha, Phys. Rev. B **79**, 085104 (2009); *ibid.* **79**, 209902 (2009) (E).

[61] C. Kittel, *Introduction to Solid State Physics* (Wiley, New York, 1986).

[62] E.G. Moroni, G. Kresse, J. Hafner, and J. Furthmuller, Phys. Rev. B **56**, 15629 (1997).

[63] P. Bagno, O. Jepsen, and O. Gunnarsson, Phys. Rev. B **40**, 1997 (1989).

[64] A.Y. Liu and D.J. Singh, Phys. Rev. B **47**, 8515 (1993).

[65] D.J. Singh, Phys. Rev. B **45**, 2258 (1992).

[66] P. Söderlind and A. Gonis, Phys. Rev. B **82**, 033102 (2010).

[67] G.L. Oliver and J.P. Perdew, Phys. Rev. A **20**, 397 (1979).

[68] C.D. Hu and D.C. Langreth, Phys. Rev.B **33**, 943 (1986).

TABLE IV: Static-lattice lattice constants, a_0 (Å), of 20 solids. The experimental values in the last column are obtained by subtracting the zero-point anharmonic expansion (ZPAE) from the experimental zero-temperature values. The experimental values of Ca, Sr, and Ba are from Ref. 7, and the rest from Ref. 38.

solids	LSDA	PBE	PBEsol	AM05	TPSS	revTPSS	Expt.
Li	3.362	3.431	3.426	3.450	3.448	3.440	3.453
Na	4.051	4.198	4.170	4.209	4.239	4.215	4.214
Ca	5.332	5.518	5.448	5.482	5.522	5.504	5.553
Sr	5.791	6.027	5.916	5.972	6.028	6.007	6.045
Ba	4.770	5.030	4.894	4.969	5.009	4.986	4.995
Al	3.983	4.035	4.011	4.001	4.008	4.005	4.018
Cu	3.522	3.633	3.565	3.563	3.580	3.559	3.595
Rh	3.759	3.831	3.781	3.774	3.805	3.785	3.794
Pd	3.844	3.942	3.876	3.870	3.904	3.884	3.876
Ag	4.002	4.145	4.050	4.051	4.086	4.052	4.062
C	3.533	3.569	3.552	3.548	3.568	3.558	3.553
SiC	4.332	4.378	4.355	4.352	4.366	4.357	4.346
Si	5.405	5.468	5.432	5.434	5.453	5.439	5.421
Ge	5.631	5.768	5.680	5.685	5.729	5.682	5.644
GaAs	5.615	5.752	5.665	5.672	5.718	5.680	5.640
LiF	3.913	4.070	4.007	4.039	4.050	4.029	3.972
LiCl	4.968	5.151	5.063	5.119	5.121	5.109	5.070
NaF	4.506	4.705	4.632	4.679	4.710	4.680	4.582
NaCl	5.467	5.695	5.603	5.678	5.701	5.667	5.569
MgO	4.170	4.261	4.223	4.229	4.244	4.240	4.189
ME	-0.082	0.051	-0.012	0.009	0.035	0.014	
MAE	0.082	0.060	0.035	0.036	0.043	0.032	
MRE(%)	-1.73	1.10	-0.24	0.19	0.73	0.29	
MARE(%)	1.73	1.29	0.73	0.75	0.90	0.68	

TABLE V: Bulk moduli, B_0 (GPa), of 20 solids. The experimental values in the last column are obtained by subtracting the zero-point phonon effects (ZPPE) from the experimental zero-temperature values. The experimental values of Ca, Sr, and Ba are from Ref. 58, and the rest from Ref. 38.

solids	LSDA	PBE	PBEsol	AM05	TPSS	revTPSS	Expt.
Li	15.1	13.8	13.7	13.2	13.3	13.4	13.9
Na	9.2	7.8	7.8	7.5	7.3	7.5	7.7
Ca	19.4	17.5	17.9	17.8	17.6	17.9	18.7
Sr	14.5	11.1	12.9	11.7	10.7	10.9	12.5
Ba	10.6	8.8	9.4	8.7	8.4	8.7	9.4
Al	83.7	77.3	81.9	86.0	85.6	85.7	82
Cu	187.4	138.0	166.0	164.0	162.4	173.8	145
Rh	315.6	256.4	295.0	296.5	281.9	296.1	272.1
Pd	226.3	169.4	205.2	203.4	195.4	209.7	198.1
Ag	138.5	90.9	118.9	114.5	110.0	120.5	110.8
C	465.8	433.2	450.2	452.0	430.3	439.5	454.7
SiC	229.5	212.8	221.9	222.1	217.2	221.5	229.1
Si	97.0	90.0	92.8	91.9	92.0	93.0	100.8
Ge	70.5	59.4	65.8	64.5	60.2	65.0	77.3
GaAs	75.1	60.5	69.9	68.3	64.8	66.8	76.7
LiF	86.7	66.9	72.2	66.4	66.2	68.9	76.3
LiCl	41.5	31.7	35.4	31.4	33.4	34.0	38.7
NaF	61.5	45.2	48.8	43.1	42.9	44.0	53.1
NaCl	31.2	23.6	26.0	22.0	22.4	24.1	27.6
MgO	172.1	149.5	157.6	154.3	155.0	155.5	169.8
ME	8.845	-10.514	-0.257	-1.754	-4.867	-0.890	
MAE	10.068	10.521	6.209	7.393	7.942	8.664	
MRE(%)	9.30	-10.52	-1.93	-5.64	-7.65	-4.26	
MARE(%)	10.77	10.61	5.69	8.94	9.65	9.04	

TABLE VI: Static-lattice cohesive energies in eV/atom of 20 solids. For Rh the decrease in the GGA's cohesive energies by 0.03-0.04 eV compared to previously published values[38,54] is related to our putting the 4s electrons in the valence and not in the core. The experimental values for Ca, Sr, and Ba are from Ref. 61, plus a small correction for zero-point vibration energy from Table V of Ref. 47. The rest of the experimental data, which have also been corrected for zero-point vibration energy, are from Ref. 38.

solids	LSDA	PBE	PBEsol	TPSS	revTPSS	Expt.
Li	1.810	1.605	1.677	1.631	1.637	1.658
Na	1.256	1.082	1.154	1.135	1.155	1.119
Ca	2.220	1.917	2.117	2.027	2.068	1.86
Sr	1.893	1.609	1.808	1.750	1.822	1.73
Ba	2.246	1.871	2.109	2.017	2.094	1.91
Al	4.038	3.438	3.817	3.478	3.570	3.431
Cu	4.545	3.474	4.027	3.787	4.121	3.524
Rh	7.563	5.688	6.642	5.776	6.155	5.783
Pd	5.016	3.714	4.435	3.981	4.379	3.938
Ag	3.642	2.516	3.078	2.733	3.034	2.985
C	9.011	7.714	8.275	7.246	7.312	7.545
SiC	**7.457**	6.401	6.876	6.189	6.255	6.478
Si	5.348	4.559	4.940	4.435	4.504	4.685
Ge	4.628	3.716	4.144	3.642	3.783	3.918
GaAs	**4.095**	3.148	3.555	3.120	3.259	3.337
LiF	**4.945**	4.322	4.474	4.223	4.228	4.457
LiCl	**3.835**	3.364	3.518	3.362	3.391	3.586
NaF	**4.384**	3.826	3.959	3.736	3.740	3.970
NaCl	**3.503**	3.097	3.223	3.104	3.137	3.337
MgO	**5.863**	4.973	5.299	4.941	4.930	5.203
ME	**0.642**	-0.121	0.234	-0.107	0.006	
MAE	**0.642**	0.144	0.253	0.173	0.206	
MRE(%)	**16.50**	-3.68	5.97	-1.99	1.22	
MARE(%)	**16.50**	4.23	6.52	4.70	5.73	

TABLE VII: Lattice constant a_0 (in Å), bulk modulus B_0 (in GPa), and magnetic moment M_0 (in μ_B) for ferromagnetic bcc Fe, nonmagnetic fcc Fe and ferromagnetic fcc Ni. δE_0 (in eV) is the difference between total energies per atom of fcc Fe and bcc Fe at each equilibrium lattice constant. A negative δE_0 indicates that the ground state is fcc. a: Ref. 44, b: Refs. 64,65, and c: Ref. 61

		LSDA	PBE	PBEsol	TPSS	revTPSS	Expt.
Fe (bcc)	a_0	2.747	2.829	2.782	2.803	2.794	2.853(2.861)[a]
	B_0	250.4	178.9	216.7	200.3	204.5	168[b]
	M_0	1.97	2.18	2.11	2.19	2.20	2.20[b]
Fe (fcc)	a_0	3.359	3.423	3.376	3.410	3.393	
	δE_0	-0.10	0.17	0.07	0.22	0.22	
Ni (fcc)	a_0	3.428	3.520	3.463	3.481	3.465	3.508(3.516)[a]
	B_0	254.5	195.6	229.3	222.3	233.4	186 [c]
	M_0	0.56	0.62	0.60	0.63	0.65	0.61 [a]